Electronic and ionic structures of warm and hot dense matter

C. E. Starrett and D. Saumon
Los Alamos National Laboratory, P.O. Box 1663, Los Alamos, New Mexico 87545, USA
(Received 25 October 2012; published 10 January 2013)

The results of a numerical implementation of the recent average atom model including ion-ion correlations of Starrett and Saumon [Phys. Rev. E **85**, 026403 (2012)] are presented. The solution is obtained by coupling an average atom model to a two-component plasma model of electrons and ions. The two models are solved self-consistently and results are given in the form of pair distribution functions. Ion-ion pair distribution functions for hydrogen, carbon, aluminum, and iron are compared to quantum and Thomas-Fermi molecular dynamics simulations as well as path-integral Monte Carlo calculations and good agreement is found for a wide variety of plasma conditions in the warm and hot dense matter regime.

DOI: 10.1103/PhysRevE.87.013104 PACS number(s): 52.27.Aj, 52.25.Jm, 52.27.Gr, 61.20.Gy

I. INTRODUCTION

Accurate modeling of hot and warm dense matter is important for understanding the cores of giant planets [1], inertial confinement fusion [2], and dense stars [3] and for simulating recent experiments in x-ray-absorption near-edge spectroscopy [4–6], x-ray Thomson scattering (XRTS) [7,8], and ionization potential depression [9]. The most powerful methods to model warm dense matter are based on *ab initio* computer simulations such as quantum and orbital-free (or Thomas-Fermi) molecular dynamics (MD), which are based on density functional theory (see, for example, Refs. [10–13]). The quantum MD method is typically limited to low temperatures (however, see Ref. [14] for some exceptions to this rule) due to increasingly prohibitive computational demands at higher temperatures. The orbital-free MD method can be used at high temperatures, but is still computationally expensive and is inaccurate at low temperatures. A drawback of orbital-free methods is that electronic wave functions are not available for the calculation of electronic transport properties [14]. Another simulation method is the path-integral Monte Carlo (PIMC) method [15], which is also computational expensive and is so far limited to high temperatures and low-Z elements such as H, He, and C [16].

Among more approximate methods to model dense ionized matter, average atom models have been quite popular. They have proved to be accurate enough to be useful while being computationally much more expedient. This last point is their central advantage over *ab initio* methods as they can be used to create large tables of material properties over a wide range of plasma conditions. This computational economy is principally the result of the assumption that the plasma is spherically symmetric about a central, fixed nucleus, which allows the angular integrals to be carried out analytically. There are, however, many different average atom models that exploit this approximation. Perhaps the most popular and successful are the Thomas-Fermi cell model [17–19] and its quantum mechanical counterpart [20,21]. Both consider an average atom at the center of a spherical cavity whose radius is the ion-sphere radius.

Recently, an average atom model was formalized using density functional theory and the integral equations of fluid theory [22], going beyond the concept of an atom in a spherical cavity by determining the ion-ion pair distribution function self-consistently and solving for the electronic response in the field created by the fixed central nucleus and the spherically averaged distribution of surrounding ions. In Ref. [22] it was suggested that the nucleus-centered system could be solved by coupling it to an ion-centered system, which allows the electron-ion and ion-ion local field corrections to be determined. However, numerical experiments have revealed that this method is accurate only for very weakly coupled systems. In the present paper an alternative method for determining the local field corrections is presented. The nucleus-centered system (the average atom model) is coupled to a two-component plasma model, consisting of classical ions and quantum electrons. By defining a neutral pseudoatom [23–25] within the average atom model, the quantum Ornstein-Zernike relations [26] for the two-component plasma (TCP) model are closed. This approach has proved to be much more successful. The TCP model is a generalization of the well-studied one-component plasma (OCP) model (see, for example, Refs. [27–29]). In the TCP model classical ions interact with each other and with a responding quantum electron fluid that screens the interactions between the ions and makes the plasma electrically neutral. This is in contrast to the OCP model, where classical ions interact with each other in a neutralizing, rigid (nonresponsive) background of electrons. Numerical comparisons between this TCP model and the OCP model are presented here.

The main goals of this paper are to present the coupling of the average atom model to the two-component plasma model and to compare numerical results in the form of ion-ion pair distribution functions to those from *ab initio* simulations. Results are presented for several elements over a wide range of plasma densities and temperatures. The inputs to the model are the nuclear charge Z, the temperature of the plasma $T = 1/\beta$, and the ion particle density n_I^0.

The ion-ion pair distribution function of warm dense matter (and the closely related structure factor) has been the subject of much interest recently in the context of XRTS experiments where it plays an essential role in the interpretation of the scattered line spectrum [8,30]. A variety of approximations to the structure factor are in use, including the hypernetted chain approximation of fluid theory with interaction potentials that are not determined consistently within the model [31] or are based on the linear response formalism coupled to charged hard spheres [30] or even based on simple fits [32].

The model presented here should prove useful in the design and analysis of XRTS experiments. Moreover, the ion-ion interaction potential found within this model can be used to calculate thermal and dc conductivities [33], which are of interest for inertial confinement fusion experiments [34] as well as diffusion coefficients.

In Sec. II the general theory of the average atom model is reviewed. This is unchanged from that of Ref. [22]. However, the notation can now be simplified because the ion-centered system is no longer considered and the theory is developed using the free energy as well as the intrinsic free energy. In Sec. III the two-component plasma model is presented and its coupling to the average atom model is shown for both quantum mechanical and semiclassical treatment of electrons. In Sec. IV calculations are presented for hydrogen, carbon, aluminum, and iron in the hot and warm dense matter regimes and compared to quantum and orbital-free MD simulations, PIMC simulations, and the OCP model as well. A summary and conclusions are presented in Sec. V. Three important issues are presented in the Appendixes. The first discusses the mapping of the two-component plasma quantum Ornstein-Zernike equations to an effective one-component system that is used in the numerical implementation of the model. The second defines a simplified version of the model based on the ion sphere with a fixed step-function pair distribution function and the third describes a method to estimate the broadening of bound states due to dense plasma effects. Unless otherwise stated, atomic units are used throughout ($\hbar = m_e = e = 1$).

II. DERIVATION OF THE AVERAGE ATOM MODEL

For a mixture of classical ions and quantum mechanical electrons in a large volume V, the grand potential Ω is related to the free energy F by

$$\Omega = F - \mu_e N_e - \mu_I N_I, \tag{1}$$

where μ_e and μ_I are the electronic and ionic chemical potentials, respectively, and N_e and N_I are the number of electrons and ions in the plasma, respectively. The free energy can be separated into three components

$$F = F^{\rm id} + F^{\rm el} + F^{\rm xc}, \tag{2}$$

where $F^{\rm id}$ is the ideal noninteracting part, $F^{\rm el}$ includes all electrostatic interactions, and $F^{\rm xc}$ is the exchange and correlation part. Another way to write the grand potential is in terms of the intrinsic free energy $\mathcal{F}$ [22],

$$\Omega = \mathcal{F} - \mu_e N_e - \mu_I N_I + \int_V d\boldsymbol{r}\, V_e(\boldsymbol{r}) n_e(\boldsymbol{r}) + \int_V d\boldsymbol{r}\, V_I(\boldsymbol{r}) n_I(\boldsymbol{r}), \tag{3}$$

where V_e is the external potential that couples to the electrons in the plasma with particle density $n_e(\boldsymbol{r})$ and similarly V_I is the external potential that couples to the ions with particle density $n_I(\boldsymbol{r})$. The intrinsic free energy can be written in two components

$$\mathcal{F} = F^{\rm id} + \mathcal{F}^{\rm ex}, \tag{4}$$

where $\mathcal{F}^{\rm ex}$ is the excess, which includes all but the noninteracting contributions. With these definitions,

$$F = \mathcal{F} + \int_V d\boldsymbol{r}[V_e(\boldsymbol{r}) n_e(\boldsymbol{r}) + V_I(\boldsymbol{r}) n_I(\boldsymbol{r})] \tag{5}$$

and

$$\mathcal{F}^{\rm ex} = F^{\rm el} + F^{\rm xc} - \int_V d\boldsymbol{r}[V_e(\boldsymbol{r}) n_e(\boldsymbol{r}) + V_I(\boldsymbol{r}) n_I(\boldsymbol{r})]. \tag{6}$$

The ideal free energy can be further separated into electron and ion terms

$$F^{\rm id} = F_e^{\rm id} + F_I^{\rm id}. \tag{7}$$

A. Ideal ion free energy

For a system of volume V, average ion density n_I^0, and temperature $T = 1/\beta$, the ideal free energy of the classical ions is

$$F_I^{\rm id}[n_I(\boldsymbol{r})] = \frac{1}{\beta}\int_V d\boldsymbol{r}\, n_I(\boldsymbol{r})[\ln|\Lambda^3 n_I(\boldsymbol{r})| - 1], \tag{8}$$

where Λ is the thermal de Broglie wavelength of an ion of mass M,

$$\Lambda = \left(\frac{2\pi\beta}{M}\right)^{1/2}. \tag{9}$$

The ion chemical potential is

$$\mu_I = \mu_I^{\rm id} + \mu_I^{\rm ex} = \frac{1}{\beta}\ln\left|\Lambda^3 n_I^0\right| + \mu_I^{\rm ex} \tag{10}$$

and the ion particle density is

$$n_I(\boldsymbol{r}) = n_I^0 \exp\left[-\beta V_I^{\rm eff}(\boldsymbol{r})\right], \tag{11}$$

where $V_I^{\rm eff}(\boldsymbol{r})$ is the effective potential in which the ions move, which will be specified later.

B. Ideal nonrelativistic quantum mechanical electron free energy

Nonrelativistic quantum mechanical electrons can be described with an effective one-electron Schrödinger equation with an effective potential $V_e^{\rm eff}(\boldsymbol{r})$,

$$\left[\hat{T} + V_e^{\rm eff}(\boldsymbol{r})\right]\psi_i(\boldsymbol{r}) = \epsilon_i\psi_i(\boldsymbol{r}), \tag{12}$$

where ϵ_i are the eigenenergies, $\psi_i(\boldsymbol{r})$ are one-electron wave functions (properly normalized according to the boundary conditions imposed; see Ref. [22] for the average atom normalization), and $\hat{T} = -\frac{1}{2}\nabla^2$ is the kinetic energy operator. The ideal part of the free energy is

$$F_e^{\rm id}[n_e(\boldsymbol{r})] = 2\int_V d\boldsymbol{r}\sum_{s\in B}[g_s\psi_s^\star(\boldsymbol{r})\hat{T}\psi_s(\boldsymbol{r}) - T\,S(g_s)|\psi_s(\boldsymbol{r})|^2] + 2\int_V d\boldsymbol{r}\frac{1}{(2\pi)^3}\int d\boldsymbol{k}\{g_k[\psi_k^\star(\boldsymbol{r})\hat{T}\psi_k(\boldsymbol{r})] - T\,S(g_k)|\psi_{\boldsymbol{k}}(\boldsymbol{r})|^2\}, \tag{13}$$

where the mean field entropy is a function of the state occupation factor

$$S(g) = -[g\ln g + (1-g)\ln(1-g)]. \tag{14}$$

The first term in Eq. (13) is the contribution from bound states B and the second term is the contribution from continuum states. The states are occupied according to Fermi-Dirac occupation factors

$$g_i = \frac{1}{\exp\left[\beta\left(\epsilon_i - \mu_e^{\rm id}\right)\right] + 1}, \tag{15}$$

where $i = s,k$ and $\mu_e^{\rm id}$ is the ideal part of the electron chemical potential. The electronic density is given by

$$n_e(\boldsymbol{r}) = 2\sum_{s\in B} g_s|\psi_s(\boldsymbol{r})|^2 + \frac{2}{(2\pi)^3}\int d\mathbf{k}\, g_k|\psi_{\mathbf{k}}(\boldsymbol{r})|^2. \tag{16}$$

For average atom models in which the potential $V_e^{\rm eff}(\boldsymbol{r})$ is spherically symmetric and short ranged, this electron density is written in a form more useful for numerical evaluation by separating the electron density into bound and continuum densities [35]

$$n_e(r) = n_e^b(r) + n_e^c(r), \tag{17}$$

where

$$n_e^b(\boldsymbol{r}) = \sum_{n,l\in B} g_n \frac{2(2l+1)}{4\pi}\left|\frac{y_{n,l}(r)}{r}\right|^2 \tag{18}$$

and

$$n_e^c(r) = \int_0^\infty d\epsilon\, g_k \sum_{l=0}^\infty \frac{2(2l+1)}{4\pi}\left|\frac{y_{k,l}(r)}{r}\right|^2, \tag{19}$$

where the wave functions ψ_i have been expanded in a complete set of spherical harmonics and the angular integrals have been evaluated analytically. Here $y_i(r)$ is the radial wave function and n and l are the principal and orbital angular momentum quantum numbers, respectively.

C. Ideal semiclassical Thomas-Fermi electron free energy

If the electrons are treated in the semiclassical Thomas-Fermi approximation, the ideal free energy is

$$F_e^{\rm id}[n_e(\boldsymbol{r})] = 2\int_V d\boldsymbol{r}\frac{1}{(2\pi)^3}\int d\boldsymbol{k}\left\{\epsilon_k g_k^{\rm TF}(\boldsymbol{r}) - TS\left[g_k^{\rm TF}(\boldsymbol{r})\right]\right\}, \tag{20}$$

where

$$g_k^{\rm TF}(\boldsymbol{r}) = \frac{1}{\exp\left\{\beta\left[\epsilon_k + V_e^{\rm eff}(\boldsymbol{r}) - \mu_e^{\rm id}\right]\right\} + 1} \tag{21}$$

and $\epsilon_k = k^2/2$. For numerical evaluation it is useful to write Eq. (20) as [36]

$$F_e^{\rm id}[n_e(\boldsymbol{r})] = \int_V \left[n_e(\boldsymbol{r})\frac{\Phi(\boldsymbol{r})}{\beta} - \frac{2}{3\beta}c_{\rm TF}I_{3/2}[\Phi(\boldsymbol{r})]\right]d\boldsymbol{r}, \tag{22}$$

where

$$c_{\rm TF} \equiv \frac{\sqrt{2}}{\pi^2\beta^{3/2}}. \tag{23}$$

The electronic density is then given by

$$n_e(\boldsymbol{r}) = c_{\rm TF}I_{1/2}[\Phi(\boldsymbol{r})], \tag{24}$$

where I_j are Fermi integrals

$$I_j(x) = \int_0^\infty \frac{y^j dy}{\exp(y-x)+1}. \tag{25}$$

For average atom models where the interaction potential is spherically symmetric and goes to zero far from the origin, the function $\Phi(\boldsymbol{r})$ can be written

$$\Phi(\boldsymbol{r}) = \beta\left[\mu_e^{\rm id} - V_e^{\rm eff}(r)\right]. \tag{26}$$

D. Average atom model

Up to now the formulation is valid for any given external potential. The average atom model is defined by letting the external potential be created by a nucleus of charge Z fixed at the origin. Then the grand potential (3) becomes

$$\Omega = \mathcal{F} - \mu_e N_e - \mu_I N_I + \int_V d\boldsymbol{r}\, V_{Ne}^C(r)n_e(\boldsymbol{r}) + \int_V d\boldsymbol{r}\, V_{NI}^C(r)n_I(\boldsymbol{r}), \tag{27}$$

where $V_{Ne}^C(r) = -Z/r$ and $V_{NI}^C(r) = ZZ^\star/r$ are the Coulomb interactions between the nucleus and the electrons and between the nucleus and ions of charge $Z^\star$, respectively.

The excess intrinsic free energy $\mathcal{F}^{\rm ex}$ can be expanded in a functional Taylor series about a reference state, chosen to be an interacting plasma of ions and electrons, where the *external* potentials are zero and the uniform electron and ion densities are n_e^0 and n_I^0, respectively. To second order in the densities, the expansion is [22]

$$\begin{aligned}\mathcal{F}^{\rm ex} = &\int_V f^{\rm ex}\left[n_e^0, n_I^0\right]d\boldsymbol{r} + \mu_e^{\rm ex}\int_V \Delta n_e(r)d\boldsymbol{r} \\ &+ \mu_I^{\rm ex}\int_V \Delta n_I(r)d\boldsymbol{r} \\ &- \frac{1}{\beta}\int_V\int_V C_{Ie}(|\boldsymbol{r}-\boldsymbol{r}'|)\Delta n_e(r)\Delta n_I(r')d\boldsymbol{r}\,d\boldsymbol{r}' \\ &- \frac{1}{2\beta}\int_V\int_V C_{II}(|\boldsymbol{r}-\boldsymbol{r}'|)\Delta n_I(r)\Delta n_I(r')d\boldsymbol{r}\,d\boldsymbol{r}' \\ &- \frac{1}{2\beta}\int_V\int_V C_{ee}(|\boldsymbol{r}-\boldsymbol{r}'|)\Delta n_e(r)\Delta n_e(r')d\boldsymbol{r}\,d\boldsymbol{r}',\end{aligned} \tag{28}$$

where $f^{\rm ex}$ is the excess free energy density of the reference state,

$$\mu_j^{\rm ex} \equiv \left.\frac{\delta\mathcal{F}^{\rm ex}}{\delta n_j(\boldsymbol{r})}\right|_{V_j=0} = \frac{\partial f^{\rm ex}}{\partial n_j^0}, \tag{29}$$

and

$$\Delta n_j(r) = n_j(r) - n_j^0 \tag{30}$$

for $j = e,I$. Neglecting higher-order terms in Eq. (28) amounts to the hypernetted chain (HNC) approximation, where bridge functions are neglected. The C_{ij} are direct correlation functions and are properties of the reference state. They are defined by

$$\frac{-1}{\beta}C_{ij}(|\boldsymbol{r}-\boldsymbol{r}'|) \equiv \left.\frac{\delta^2\mathcal{F}^{\rm ex}}{\delta n_i(\boldsymbol{r})\delta n_j(\boldsymbol{r}')}\right|_{V_i=0} \tag{31}$$

and can be written in terms of a Coulomb interaction $V_{ij}^C(r)$ and an exchange and correlation interaction (in Fourier space)

$$C_{ij}(k) = -\beta V_{ij}^C(k) + \tilde{C}_{ij}(k), \tag{32}$$

where

$$\tilde{C}_{ij}(k) = \beta V_{ij}^C(k) G_{ij}(k), \tag{33}$$

which defines the local field corrections (LFCs) $G_{ij}(k)$. Using Eqs. (32), (28), and (27), the grand potential and free energy can be written in the alternative form of Eqs. (1) and (2), where the purely Coulombic free energy is

$$\begin{aligned} F^{\rm el} = &\int_V d\boldsymbol{r}\, V_{Ne}^C(r) n_e(r) + \int_V d\boldsymbol{r}\, V_{NI}^C(r) n_I(r) \\ &+ \int_V \int_V V_{Ie}^C(|\boldsymbol{r}-\boldsymbol{r}'|) n_e(r) n_I(r') d\boldsymbol{r}\, d\boldsymbol{r}' \\ &+ \frac{1}{2}\int_V \int_V V_{II}^C(|\boldsymbol{r}-\boldsymbol{r}'|) n_I(r) n_I(r') d\boldsymbol{r}' d\boldsymbol{r} \\ &+ \frac{1}{2}\int_V \int_V V_{ee}^C(|\boldsymbol{r}-\boldsymbol{r}'|) n_e(r) n_e(r') d\boldsymbol{r}' d\boldsymbol{r} \end{aligned} \tag{34}$$

and the exchange-correlation term is

$$\begin{aligned} F^{\rm xc} = &-\frac{1}{\beta}\int_V \int_V \tilde{C}_{Ie}(|\boldsymbol{r}-\boldsymbol{r}'|) \\ &\times \left[\Delta n_e(r) - n_e^{\rm ion}(r)\right] \Delta n_I(r') d\boldsymbol{r}' d\boldsymbol{r} \\ &- \frac{1}{2\beta}\int_V \int_V \tilde{C}_{II}(|\boldsymbol{r}-\boldsymbol{r}'|) \Delta n_I(r) \Delta n_I(r') d\boldsymbol{r}' d\boldsymbol{r} \\ &+ F_{ee}^{\rm xc}[n_e(r)] + F_{Ie}^c\left[n_e^0, n_I^0\right] + F_{II}^c\left[n_I^0\right]. \end{aligned} \tag{35}$$

The LFCs of electron-electron exchange and correlations are evaluated within the local density approximation. Also, as in Ref. [22], electron-ion correlations for ion core states [with electron density $n_e^{\rm ion}(r)$] have been explicitly set to zero by removing these states in Eq. (35). Note that Eq. (34) is written in terms of $n_j(r)$ $(j = e, I)$ rather than $\Delta n_j(r)$. This is a more intuitive form for the electrostatic energy, however it is easy to show that both forms are equal.

Global neutrality requires that the total charge of the system be zero; then

$$Z = \int_V [n_e(r) - Z^\star n_I(r)] d\boldsymbol{r}. \tag{36}$$

Since the interaction of the nucleus with the surrounding electrons and ions is screened, it will be short ranged. The electronic and ionic densities will therefore go to their free particle limits far from the origin,

$$\lim_{r\to\infty} n_e(r) = n_e^0, \tag{37}$$

$$\lim_{r\to\infty} n_I(r) = n_I^0; \tag{38}$$

therefore the average atom (AA) ion charge is

$$Z^\star = \frac{n_e^0}{n_I^0}. \tag{39}$$

Note that this does not determine $Z^\star$ since n_e^0 is also unknown *a priori*. The latter is related to the ideal part of the electron chemical potential $\mu_e^{\rm id}$ [22] by setting $V_e^{\rm eff}(r) = 0$ in Eq. (23):

$$n_e^0 = c_{\rm TF} I_{1/2}\left(\beta \mu_e^{\rm id}\right). \tag{40}$$

For the calculations presented here $\mu_e^{\rm id}$ is calculated with a model presented in Appendix B. In principle, $\mu_e^{\rm id}$ can be determined within the full model, either using an additional neutrality condition [37] or through a variational principle [22]. This will not be addressed in the present paper.

E. Minimization of the grand potential

Given the above approximation to the grand potential Ω, we follow the principles of density functional theory by minimizing Ω with respect to particle densities:

$$\frac{\delta\Omega}{\delta n_e(r)} = 0 \tag{41}$$

and

$$\frac{\delta\Omega}{\delta n_I(r)} = 0. \tag{42}$$

Differentiating the various contributions to Ω, we have

$$\frac{\delta F_e^{\rm id}}{\delta n_e(r)} = \mu_e^{\rm id} - V_{Ne}^{\rm eff}(r), \tag{43}$$

which is correct for both the quantum and semiclassical formulas (13) and (20),

$$\frac{\delta F_I^{\rm id}}{\delta n_I(r)} = \mu_I^{\rm id} - V_{NI}^{\rm eff}(r), \tag{44}$$

and

$$\frac{\delta F^{\rm el}}{\delta n_e(r)} = V_{Ne}^{\rm el}(r), \tag{45}$$

$$\frac{\delta F^{\rm el}}{\delta n_I(r)} = V_{NI}^{\rm el}(r) = -Z^\star V_{Ne}^{\rm el}(r), \tag{46}$$

where

$$V_{Ne}^{\rm el}(r) = V_{Ne}^C(r) + \int d\boldsymbol{r}' \frac{n_e(r') - Z^\star n_I(r')}{|\boldsymbol{r}-\boldsymbol{r}'|}, \tag{47}$$

and

$$\frac{\delta F^{\rm xc}}{\delta n_e(r)} = V_{ee}^{\rm xc}[n_e(r)] + V_{Ie}^{e,c}[n_I(r)], \tag{48}$$

$$\frac{\delta F^{\rm xc}}{\delta n_I(r)} = V_{II}^c[n_I(r)] + V_{Ie}^{I,c}[n_e(r)], \tag{49}$$

where

$$V_{ee}^{\rm xc}[n_e(r)] \equiv \frac{\delta F_{ee}^{\rm xc}}{\delta n_e(r)}, \tag{50}$$

$$V_{Ie}^{e,c}[n_I(r)] \equiv -\frac{1}{\beta}\int \tilde{C}_{Ie}(|\boldsymbol{r}-\boldsymbol{r}'|) \Delta n_I(r') d\boldsymbol{r}', \tag{51}$$

$$\begin{aligned} V_{Ie}^{I,c}[n_e(r)] \equiv &-\frac{1}{\beta}\int \tilde{C}_{Ie}(|\boldsymbol{r}-\boldsymbol{r}'|) \\ &\times \left[\Delta n_e(r') - n_e^{\rm ion}(r')\right] d\boldsymbol{r}', \end{aligned} \tag{52}$$

and

$$V_{II}^c[n_I(r)] \equiv -\frac{1}{\beta}\int \tilde{C}_{II}(|\boldsymbol{r}-\boldsymbol{r}'|) \Delta n_I(r') d\boldsymbol{r}'. \tag{53}$$

Applying the variational principle (41), the effective electron-nucleus potential is found to be

$$V_{Ne}^{\rm eff}(r) = V_{Ne}^{\rm el}(r) + V_{ee}^{\rm xc}[n_e(r)] - V_{ee}^{\rm xc}\left[n_e^0\right] + V_{Ie}^{e,c}[n_I(r)] \tag{54}$$

and Eq. (42) yields the effective ion-nucleus potential

$$V_{NI}^{\rm eff}(r) = -Z^{\star} V_{Ne}^{\rm el}(r) + V_{II}^{c}[n_I(r)] + V_{Ie}^{I,c}[n_e(r)]. \quad (55)$$

This defines the average atom model. Equations (54) and (55) are solved together with Eqs. (11) and (17) [or Eq. (24) for semiclassical electrons] with $V_I^{\rm eff}(r) = V_{NI}^{\rm eff}(r)$ and $V_e^{\rm eff}(r) = V_{Ne}^{\rm eff}(r)$. The inputs are Z, n_I^0, and β (with $\mu_e^{\rm id}$ given by the corresponding ion-sphere model defined in Appendix B). Approximations are also required for the electron exchange and correlation potential $V_{ee}^{\rm xc}$ [Eq. (50)] and for the LFCs that appear in the correlations potentials $V_{Ie}^{e,c}$, $V_{Ie}^{I,c}$, and V_{II}^{c}. Here $V_{ee}^{\rm xc}$ is chosen to be the zero-temperature Dirac exchange functional [38], which is sufficient for the present purposes. Although more sophisticated approximations are available, a systematic study of the quantitative effect of the exchange-correlation functional on the model is beyond the scope of this paper. The ion-ion and ion-electron LFCs are found by coupling this average atom model to a two-component plasma model, which is described in the following section.

III. TWO-COMPONENT PLASMA MODEL

The electron-ion and ion-ion LFCs (G_{Ie} and G_{II}, respectively) that appear in the correlation potentials (51)–(53) are evaluated in the framework of the integral equation theory of interacting fluids. The quantum Ornstein-Zernike (QOZ) equations [22,26,39] are solved for a system of classical ions or nuclei of average density n_I^0 and quantum electrons of average density $\bar{n}_e^0$. The reason for introducing a different electron density $\bar{n}_e^0$ will become clear below. In Fourier space

$$h_{II}(k) = C_{II}(k) + n_I^0 C_{II}(k) h_{II}(k) + \bar{n}_e^0 C_{Ie}(k) h_{Ie}(k), \quad (56)$$

$$h_{Ie}(k) = -\frac{\chi_{ee}^0(k)}{\bar{n}_e^0 \beta}\big[C_{Ie}(k) + n_I^0 C_{Ie}(k) h_{II}(k) + \bar{n}_e^0 C_{ee}(k) h_{Ie}(k)\big]. \quad (57)$$

The $h_{ij}(r)$ are pair correlation functions and the $h_{ij}(k)$ are their Fourier transform

$$h_{ij}(k) = \frac{4\pi}{k}\int_0^{\infty} r h_{ij}(r)\sin(kr)\,dr. \quad (58)$$

The quantum nature of the electrons is embodied in $\chi_{ee}^0(k)$, which is the response function for a homogeneous, noninteracting quantum mechanical electron fluid. In the classical limit $\chi_{ee}^0(k) = -\bar{n}_e^0\beta$ and the classical Ornstein-Zernike equations for a binary mixture are recovered [40]. At zero temperature χ_{ee}^0 is the well-known Lindhard function [41], which has also been extended to finite temperatures [42].

This system of ions and electrons is a different model for the plasma than the average atom model. Here a system of identical point *ions* with an accompanying cloud of screening electrons interact with each other. In the average atom model a single *nucleus* is surrounded by a spherically averaged system of interacting electrons and ions. It is assumed that the LFCs obtained by solving the QOZ relations are the correct LFCs for the average atom model. This is a reasonable assumption since both approaches model the same plasma under the same conditions and, as will be shown below, they are coupled in a single model.

The QOZ system can be thought of as a two-component (electrons and ions) generalization of the well-studied OCP model (see, for example, Refs. [27–29]). The OCP model is an idealized plasma model where classical ions interact with each other with a Coulomb potential, in a rigid (nonresponding) background of negative charge that neutralizes the system. In the TCP model the classical ions interact with the quantum mechanical (or semiclassical) electrons, which in turn respond to the presence of the ions. The TCP model based on the QOZ equations (56) and (57) recovers the OCP formulation in terms of integral equations by setting the electron-ion interaction to zero ($C_{Ie} = 0$).

The QOZ equations (56) and (57) constitute two equations with five unknowns (h_{II}, h_{Ie}, C_{II}, C_{Ie}, and C_{ee}). Three additional relations are required to solve for the structure of the TCP model. For the calculations presented in this paper the direct correlation function C_{ee} is obtained from the jellium model [39]. This approximation greatly simplifies the general problem at the cost of introducing a new difficulty. Since the jellium is a model for an interacting quantum fluid of electrons in a uniform, neutralizing positive background charge, it is a poor approximation for a system where electrons can form bound states with nuclei and thus correlate very strongly with the positions of the nuclei. Therefore, the jellium model approximation for C_{ee} is not appropriate in the QOZ relations for a mixture of nuclei and electrons since in general this would involve the formation of highly correlated bound states. This forces the consideration of a different TCP model that consists of a mixture of ions and screening electrons, where the most strongly correlated (e.g., bound) electrons are incorporated in the ion (to be defined) and the direct correlation function of the remaining electrons C_{ee} can be approximated with that of the jellium.[1]

A second expression is provided by the so-called closure relation for the ions

$$g_{II}(r) \equiv h_{II}(r) + 1 = \exp\big[-\beta V_{II}^{\rm eff}(r)\big], \quad (59)$$

where

$$-\beta V_{II}^{\rm eff}(r) = -\beta V_{II}^{C}(r) + h_{II}(r) - C_{II}(r) + B_{II}(r), \quad (60)$$

$g_{II}(r)$ is the ion-ion pair distribution function, and $B_{II}(r)$ is the ion-ion bridge function, which includes all ion-ion correlations beyond two-particle correlations. The exact bridge function is unknown in general, but can be approximated in several ways [40,43–46]. For point ions of charge $\bar{Z} = \bar{n}_e^0/n_I^0$, $V_{II}^{C}(r) = \bar{Z}^2/r$ is the Coulomb interaction. For the calculations presented here, the bridge function should not be too important and it is set to $B_{II}(r) = 0$. This is the HNC approximation. The bridge function will become important as ion-ion correlations become very strong at lower temperatures ($T \lesssim 1$ eV), such as in liquid metals.

The final relation (the ion-electron closure relation) is provided by coupling the QOZ relations to the average atom

[1] It is for this reason that the ion states have to be explicitly removed from the average atom electron-ion correlation potential and free energy [Eqs. (35) and (52)].

model. There are several ways to achieve this. The method proposed in Ref. [22] relies upon calculating the electron distribution around a point ion, whose charge is given by the average atom ion charge $Z^\star$, which is then used to give h_{Ie}. This turns out to be a poor approximation except for very weakly coupled, fully ionized cases. Indeed, for cases where bound states are present, it is often impossible to find a solution using that method. It fails because the electron distribution around a point ion is in general a poor approximation to the electron distribution around a nucleus with bound states that constitutes the ion. Moreover, the constraint that the AA ion charge $Z^\star$ be the same as the TCP ion charge $\bar{Z}$ is both unnecessary and generally unjustified on physical grounds. The electron-ion closure relation used in Ref. [26] does take into account the effect of the bound states and nucleus that constitute the ion on h_{Ie}, but again overconstrains the model by imposing $Z^\star = \bar{Z}$. However, there is a much better approximation, which we now describe.

The QOZ equations can be rewritten [47]

$$S_{II}(k) = 1 + n_I^0 h_{II}(k) = \frac{1 + \chi_{ee}^0(k) C_{ee}(k)/\beta}{D(k)}, \quad (61)$$

$$S_{Ie}(k) = \sqrt{\bar{n}_e^0 n_I^0}\, h_{Ie}(k) = -\sqrt{\frac{n_I^0}{\bar{n}_e^0}}\, \chi_{ee}^0(k) \frac{C_{Ie}(k)}{\beta D(k)}, \quad (62)$$

$$\chi_{ee}(k) = \chi_{ee}^0(k) \frac{1 - n_I^0 C_{II}(k)}{D(k)}, \quad (63)$$

where

$$D(k) \equiv \left[1 - n_I^0 C_{II}(k)\right]\left[1 + \chi_{ee}^0(k) C_{ee}(k)/\beta\right] + n_I^0 \chi_{ee}^0(k) |C_{Ie}(k)|^2/\beta \quad (64)$$

and $\chi_{ee}(k)$ is the response function of the interacting electrons. The S_{ij} are the static structure factors [39], which are related to the pair correlation functions

$$S_{ij}(k) = \delta_{ij} + \sqrt{n_i^0 n_j^0}\, h_{ij}(k). \quad (65)$$

From Eqs. (61) and (62)

$$S_{Ie}(k) = \sqrt{\frac{n_I^0}{\bar{n}_e^0}}\, S_{II}(k) n_e^{\rm scr}(k), \quad (66)$$

which defines an electron density

$$n_e^{\rm scr}(k) \equiv \frac{-\chi_{ee}^0(k) C_{Ie}(k)/\beta}{1 + \chi_{ee}^0(k) C_{ee}(k)/\beta}. \quad (67)$$

Rewriting Eq. (66) in real space and in terms of pair distribution functions $g_{ij}(r) \equiv h_{ij}(r) + 1$,

$$\bar{n}_e^0 g_{Ie}(r) = n_e^{\rm scr}(r) + n_I^0 \int d\boldsymbol{r}'\, g_{II}(|\boldsymbol{r} - \boldsymbol{r}'|) n_e^{\rm scr}(r') \quad (68)$$

and

$$\bar{n}_e^0 g_{Ie}(r) = \bar{n}_e(r), \quad (69)$$

$$n_I^0 g_{II}(r) = \bar{n}_I(r), \quad (70)$$

where $\bar{n}_e(r)$ is the electron density of all screening electrons (for all ions) and $\bar{n}_I(r)$ is the ionic density, it is seen that $n_e^{\rm scr}$ can be interpreted as the screening cloud of electrons that surrounds each ion in the plasma [26]. New symbols for the ion and electron densities in the TCP model distinguish them from those of the average atom system. Using the Percus trick [48], the latter are given by

$$n_e(r) = n_I^0 Z g_{Ne}(r), \quad (71)$$

$$n_I(r) = n_I^0 g_{NI}(r). \quad (72)$$

Equation (71) defines $g_{Ne}(r)$ from the electron density $n_e(r)$ obtained by Eq. (17). These densities minimize the grand potential [Eqs. (41) and (42)]. In general, $g_{NI}(r) \neq g_{II}(r)$ and $g_{Ne}(r) \neq g_{Ie}(r)$. The electron density $\bar{n}_e(r)$ includes all electrons surrounding all ions in the plasma, whereas in the average atom system $n_e(r)$ includes the electrons surrounding the central nucleus as well as the free electrons that surround the ions. This is a key distinction: $\bar{n}_e(r)$ represents electrons in the weaker field due to the ions, while $n_e(r)$ includes electrons in the stronger field surrounding the central nucleus and *field-free* electrons surrounding the ions. The consequence is that $\bar{n}_e^0 \neq n_e^0$ in general. Here $\bar{n}_e^0$ is given by

$$\int d\boldsymbol{r}\, n_e^{\rm scr}(r) = \frac{\bar{n}_e^0}{n_I^0} = \bar{Z}. \quad (73)$$

As already noted, this distinction was not exploited in Ref. [22] or in Ref. [26].

It is now necessary to define what constitutes an ion in the AA and TCP models, which is to a certain extent arbitrary. We use the neutral pseudoatom approach [23–25] in which a pseudoatom electron density $n_e^{\rm pa}(r)$ is found by solving for the electronic density in the full average atom system, with some distribution of ions, and removing from it the electron density for a system with the same distribution of ions, but no central nucleus, $n_e^{\rm ext}(r)$ (see Appendix B)

$$n_e^{\rm pa}(r) = n_e(r) - n_e^{\rm ext}(r). \quad (74)$$

Note that by definition

$$\int d\boldsymbol{r}\, n_e^{\rm pa}(r) = Z. \quad (75)$$

The screening cloud of electrons is defined by removing the electron density due to the ion bound states $n_e^{\rm ion}(r)$ from $n_e^{\rm pa}(r)$,

$$n_e^{\rm scr}(r) = n_e^{\rm pa}(r) - n_e^{\rm ion}(r). \quad (76)$$

The problem is now to define $n_e^{\rm ion}(r)$. For the Thomas-Fermi (TF) treatment of the electrons we have used the definition of Ref. [49]

$$\begin{aligned} n_e^{\rm ion}(r) &= c_{\rm TF}\Big(I_{1/2}\left\{\beta\left[\mu_e^{\rm id} - V_{Ne}^{\rm eff}(r)\right]\right\} \\ &\quad - J_{1/2}\left\{\beta\left[\mu_e^{\rm id} - V_{Ne}^{\rm eff}(r)\right], -\beta V_{Ne}^{\rm eff}(r)\right\}\Big) \quad \text{for } r < R_0 \\ &= 0 \quad \text{for } r > R_0, \end{aligned} \quad (77)$$

where R_0 is the first zero of $V_{Ne}^{\rm eff}(r)$ and $J_{1/2}$ is the incomplete Fermi integral

$$J_{1/2}(x,a) = \int_a^\infty \frac{y^{1/2} dy}{\exp(y - x) + 1}. \quad (78)$$

Thus $n_e^{\rm ion}(r)$ includes all electrons with negative energy that are within $r \leqslant R_0$. Electrons with negative energy and $r > R_0$ are attributed to the other ions in the system. For the quantum

case the electron density of an ion is defined as

$$n_e^{\rm ion}(r) = 2\sum_{s\in B} g_s |\psi_s(\boldsymbol{r})|^2 M(\epsilon_s) f^{\rm cut}(r), \tag{79}$$

where $f^{\rm cut}(r)$ is a radial cutoff function [23]

$$f^{\rm cut}(r) = \frac{1+e^{-1/c}}{1+e^{(r-R)/cR}}, \tag{80}$$

with R the ion-sphere radius and c a constant that is taken to be $c = 0.05$. The purpose of this cutoff function is to remove long-range tails in the bound-state electron density from the screening cloud $n_e^{\rm scr}$. As discussed in Ref. [23], these long-range tails should be attributed to the noncentral ions. This is effectively the same physical idea as the cutoff radius R_0 in the definition of the TF ion density (77). Here $M(\epsilon)$ is a level occupation fraction introduced to ensure a continuous definition for $n_e^{\rm ion}(r)$ when a bound state ionizes or recombines. In the AA model bound states are discrete eigenvalue states. In a real plasma bound states are broadened in energy as they move closer to the continuum of electrons; the broadening is caused by dense plasma effects: the overlap of wave functions and the nonspherical symmetry of the plasma around an ion, both of which are missing from the AA model. This effect can be emulated in a simple way by giving each bound state of eigenenergy $\epsilon < 0$ a weight $0 \leqslant M(\epsilon) \leqslant 1$ that gives the probability that the state has moved into the continuum ($\epsilon \geqslant 0$) and that is implicitly a function of density and temperature. Assuming that the broadening takes a Gaussian shape with a full width at half maximum of γ, the broadening width γ is estimated from the average collision time of electron scattering states (Appendix C). The weight $M(\epsilon)$ is then defined as the fraction of the broadened Gaussian profile that is still "bound," i.e., with $\epsilon < 0$,

$$M(\epsilon) \equiv \mathrm{erf}\left(\frac{-2\sqrt{\ln 2}\epsilon}{\gamma}\right), \tag{81}$$

where erf is the error function. For a deeply bound state, $-\epsilon \gg \gamma$, $M \to 1$, and the broadening has no effect. For a state that just entered the continuum, $M(\epsilon = 0) = 0$ and it no longer contributes to $n_e^{\rm ion}(r)$. The electron density of an ion defined by Eq. (79) is a continuous function of density and temperature as bound states gradually move into the continuum or recombine with the ion. These corrections to $n_e^{\rm ion}(r)$ only affect the results under conditions where a state crosses into the continuum. Examples for eigenvalues, broadening widths, and the corresponding state occupation factor for solid density aluminum are given in Table I. At temperatures of 2 and 15 eV the core states $1s$, $2s$, and $2p$ are deeply bound and the corresponding occupation factor $M(\epsilon) = 1$. These states fully contribute to $n_e^{\rm ion}(r)$. However, at 2 eV the $3s$ state is unbound, whereas it is weakly bound at 15 eV with $\gamma \gg |\epsilon|$. Correspondingly $M(\epsilon_{3s}) < 1$ and the state is partially bound.

The screening densities $n_e^{\rm scr}(r)$ for these two cases are shown in Fig. 1 for both the quantum mechanical and semiclassical treatments of the electrons. The oscillations seen in the quantum calculations near the origin arise from the orthogonality of the free states contributing to $n_e^{\rm scr}(r)$ to the bound states in $n_e^{\rm ion}(r)$. The small bump at $r \sim 1.1R$ in the 15-eV calculation is a consequence of the weakly bound $3s$ state (Table I). The Friedel oscillations that are clearly seen at 2 eV in the quantum case disappear at 15 eV, as expected. Friedel oscillations do not appear in the semiclassical calculations. While the semiclassical $n_e^{\rm scr}(r)$ is a poor approximation of the quantum result at 2 eV, it becomes a more reliable approximation at higher temperature.

TABLE I. Eigenvalues ϵ, weighting factors $M(\epsilon)$, and broadening widths γ for Al at 2.7 g/cm^3 and two temperatures. The $3s$ state is not bound at $T = 2$ eV. Here ϵ and γ are in hartrees.

	$T = 2$ eV		$T = 15$ eV	
State	ϵ	$M(\epsilon)$	ϵ	$M(\epsilon)$
$1s$	−54.6	1.00	−54.9	1.00
$2s$	−3.41	1.00	−3.60	1.00
$2p$	−2.04	1.00	−2.23	1.00
$3s$			−0.0125	0.134
		γ		
	0.0698		0.174	

IV. RESULTS

In summary, an average atom model in which the distribution of ions is calculated self-consistently with the electron distribution has been derived. The AA model requires local field corrections, which describe the correlations between the electrons and ions and between the ions and ions. These LFCs are obtained by coupling the AA model to a

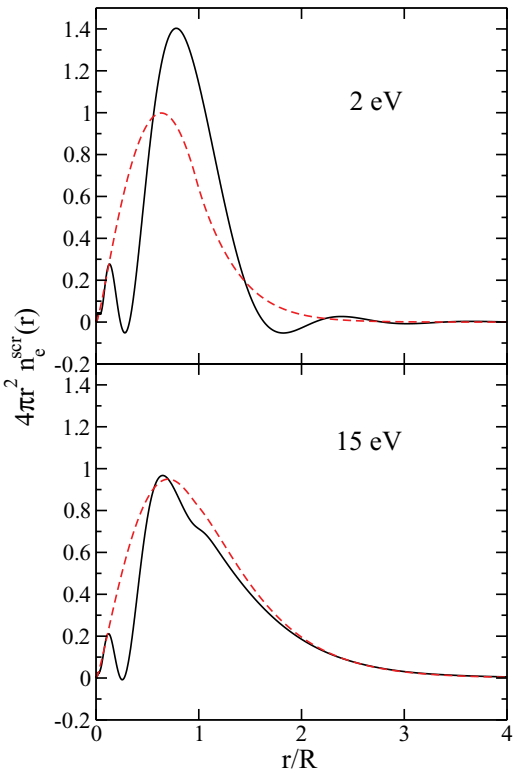

FIG. 1. (Color online) Screening electron density $n_e^{\rm scr}(r)$ for Al at solid density (2.7 g/cm^3) and two temperatures. Solid lines, quantum mechanical electrons; dashed lines, semiclassical (Thomas-Fermi) electrons. The ion sphere radius is $R = 2.99$ a.u.

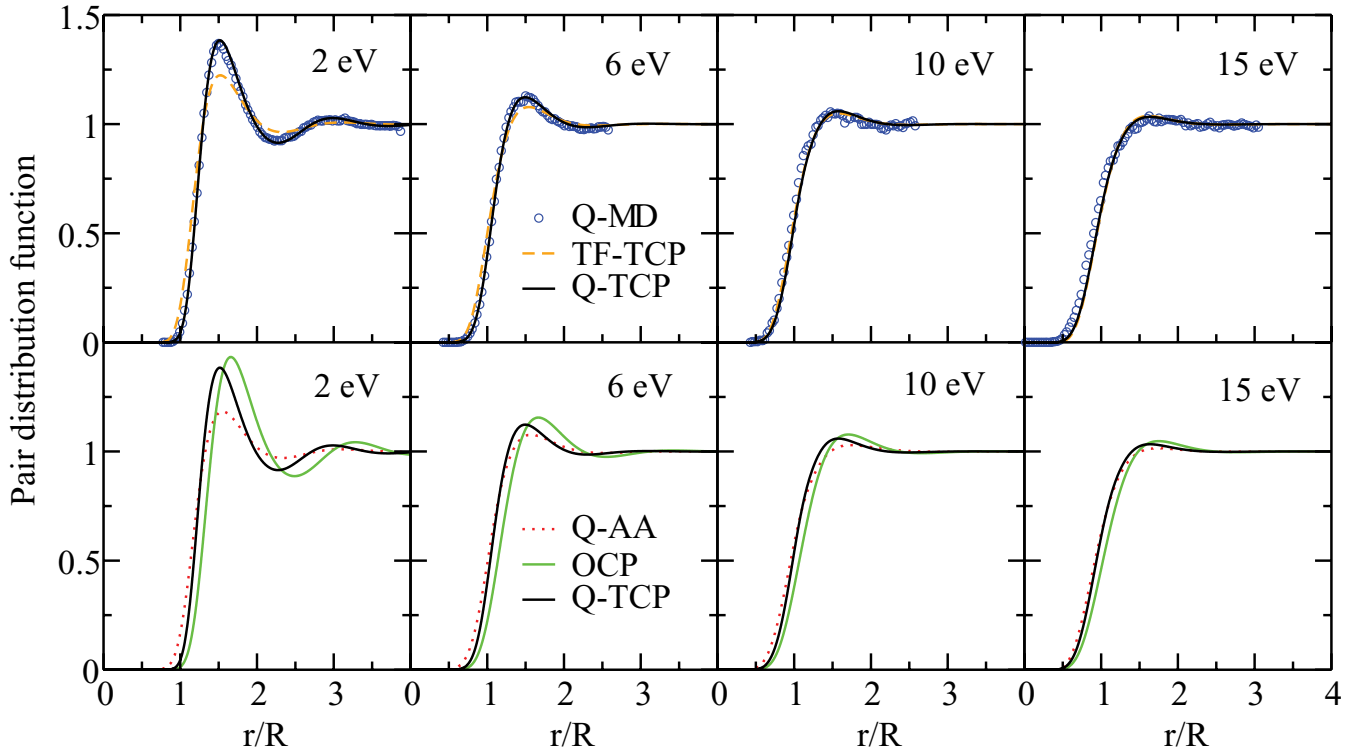

FIG. 2. (Color online) Pair distribution functions $g_{II}(r)$ for Al at solid density (2.7 g/cm^3) and $T = 2$–15 eV. The curves labeled QAA show $g_{NI}(r)$ from the average atom model. The $g_{II}(r)$ of the TFTCP and QTCP models are essentially identical at 10 and 15 eV. The QMD results are from Ref. [50]. The ion sphere radius is $R = 2.99$ a.u.

two-component plasma model. The AA model provides a closure relation for the TCP model. In turn the TCP model provides the LFCs for the AA model. The equations for the two models are solved self-consistently by numerical iteration until convergence is achieved. The numerical solution of this set of coupled, highly nonlinear equations is a nontrivial exercise. The system of equations was solved for a wide range of densities, temperatures, and elements, treating the electrons both quantum mechanically and semiclassically. The results are presented in terms of the ion-ion pair distribution function $g_{II}(r)$, which can be readily compared to those obtained from *ab initio* simulations.

In Fig. 2, $g_{II}(r)$ for aluminum at solid density is shown for $T = 2$–15 eV. Results obtained with the quantum two-component plasma model (QTCP) should be compared to the quantum molecular dynamics (QMD) simulations [50]. For all temperatures the agreement between these models is very good. As expected, the TCP model with Thomas-Fermi electrons (the TFTCP model) agrees with the quantum mechanical calculations at the higher temperatures ($T \geqslant 10$ eV), but is progressively worse at lower temperatures. It is well known that the TF approximation smooths the electronic shell structure of bound states. The latter becomes important for the lower temperature cases presented in Fig. 2, as demonstrated in Fig. 1. It is interesting that the $3s$ state, which is weakly bound and partially occupied at $T = 15$ eV (see Table I), does not detrimentally affect the agreement of $g_{II}(r)$ for the quantum cases, indicating that the definitions of the occupation fraction (81) and cutoff function (80) are reasonable. The $3s$ state is also partially bound at 10 eV [$M(\epsilon_{3s}) = 0.097$], where good agreement is also found.

The one-component plasma is a well-studied limiting model for dense plasmas whose structure factor is often used as an approximation for more complex ionized fluids. The pair distribution function $g_{II}(r)$ for the OCP (Fig. 2) was computed in the HNC approximation (as are the QTCP calculations) using the method of Ref. [27]. The OCP is characterized by a single parameter, the plasma coupling parameter, defined as the ratio of the electrostatic potential energy of two neighboring ions of charge Z to their kinetic energy

$$\Gamma_{\rm OCP} = \frac{Z^2}{RkT}, \tag{82}$$

where R is the ion-sphere radius. The OCP calculations presented here use the ion charge $Z = \bar{Z}$ from the QTCP calculation [Eq. (73)] given in Table II. This allows us to isolate the effect of electron screening, present in the TCP model but not in the OCP model. In comparison with the QTCP, the first

TABLE II. Parameters corresponding to the calculations shown in Fig. 2 for Al at 2.7 g/cm^3 ($n_I^0 = 8.93 \times 10^{-3}$).

T (eV)	$Z^\star$	$\bar{Z}$	$\Gamma_{\rm OCP}$	$\Gamma_{\rm TCP}$
2	1.98	3.00	41.0	5.05
6	2.11	3.00	13.6	2.04
10	2.24	3.00	8.14	1.60
15	2.51	3.18	6.12	1.34

TABLE III. Parameters corresponding to the calculations shown in Fig. 5 for Fe along the principal Hugoniot.

ρ (g/cm^3)	n_I^0	T (eV)	$Z^\star$	$\bar{Z}$	$\Gamma_{\rm OCP}$	$\Gamma_{\rm TCP}$
22.5	0.0360	10	5.85	8.78	112	14.3
34.5	0.0551	100	9.54	11.6	22.4	4.85
39.65	0.0634	1000	20.4	21.7	8.22	3.32
34.37	0.0549	5000	25.1	25.5	2.18	1.35

peak of the OCP $g_{II}(r)$ is systematically higher and shifted to a larger radius. The ion-ion interaction in the OCP models is purely Coulombic, which is everywhere more repulsive than the screened $V_{II}^{\rm eff}(r)$ of the QTCP model. Defining a TCP coupling parameter in analogy with Eq. (82),

$$\Gamma_{\rm TCP} = \frac{V_{II}^{\rm eff}(r=R)}{kT}, \tag{83}$$

the relative magnitude in $\Gamma_{\rm TCP}$ to $\Gamma_{\rm OCP}$ gives an indication of the importance of screening effects. The values of these coupling parameters are given in Table II for the cases presented in Fig. 2. At 2 eV $\Gamma_{\rm OCP}/\Gamma_{\rm TCP} = 8.12$, while at 15 eV $\Gamma_{\rm OCP}/\Gamma_{\rm TCP} = 4.57$, indicating that screening is more significant at lower T, as expected. However, the change in this ratio with temperature is relatively weak and so the error in neglecting electron screening in the OCP is roughly constant;

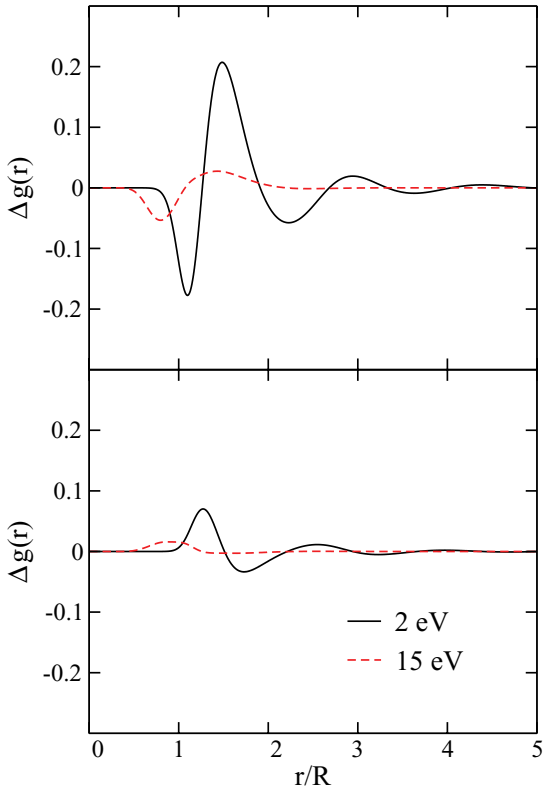

FIG. 3. (Color online) Top: Difference between the QTCP ion-ion pair distribution function and the QAA nucleus-ion pair distribution function $\Delta g(r) = g_{II}(r) - g_{NI}(r)$. Bottom: Difference between the QTCP model and the approximate guess of $g_{II}(r)$ used to initialize the iterative solution of the QTCP model (Appendix B). The examples shown are for aluminum at solid density (2.7 g/cm^3).

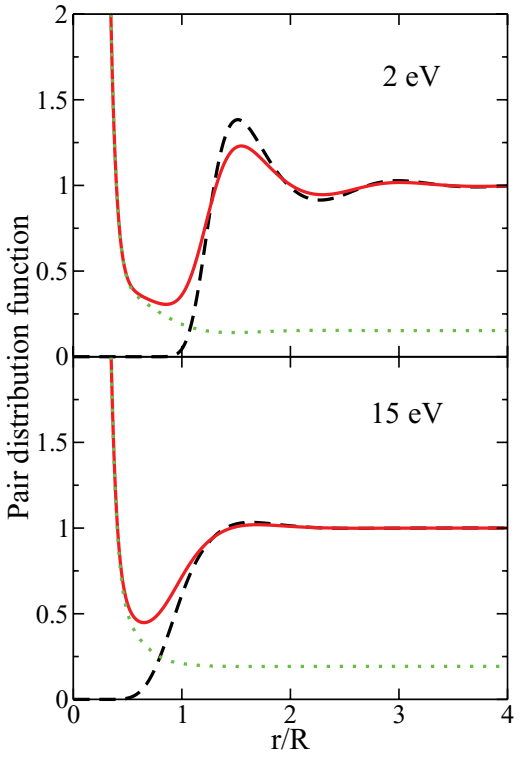

FIG. 4. (Color online) Pair distribution functions for aluminum at solid density (2.7 g/cm^3). Black (dashed) line, QTCP $g_{II}(r)$; red (solid) line, QTCP $g_{Ne}(r)$ [Eq. (84)]; green (dash-dotted) line, QAA $g_{Ne}(r)$. The ion sphere radius is $R = 2.99$ a.u.

this explains why the shift seen in the OCP $g_{II}(r)$ relative to the TCP $g_{II}(r)$ does not change significantly over the temperature range seen.

The nucleus-ion pair distribution function $g_{NI}(r)$ [Eq. (72)] of the average atom model with quantum mechanical electrons (the QAA model) is also shown in Fig. 2. As expected, it is not identical to $g_{II}(r)$, but similar. Typically it shows less correlation (peak heights are suppressed) than the corresponding QTCP calculation and becomes closer to $g_{II}(r)$ for higher temperatures. Both effects are explained by the fact that, as seen in Table II, the average atom ion charge is less than the TCP ion charge ($Z^\star < \bar{Z}$) and that for higher temperatures the two ionic charges become more similar (Table II). These two ionic charges are not expected to be the same as they correspond to different electronic densities, as discussed in Sec. III. Moreover, the QAA pair distribution $g_{NI}(r)$ is not expected to be the same as the QTCP or QMD $g_{II}(r)$ as they represent distribution functions around a nucleus and around an ion, respectively. This distinction is highlighted in Fig. 3, where differences in pair distribution functions are plotted for aluminum at solid density and two temperatures. The top panel shows the difference between the QTCP $g_{II}(r)$ and the QAA $g_{NI}(r)$. The difference decreases with temperature and is largest in the region in and around the first peak of $g_{II}(r)$. The bottom panel is the difference in the fully self-consistent QTCP g_{II} and the initial guess using the screening density from the quantum version of the ion-sphere model (Appendix B). In all the cases studied here, this simplified model provides a very

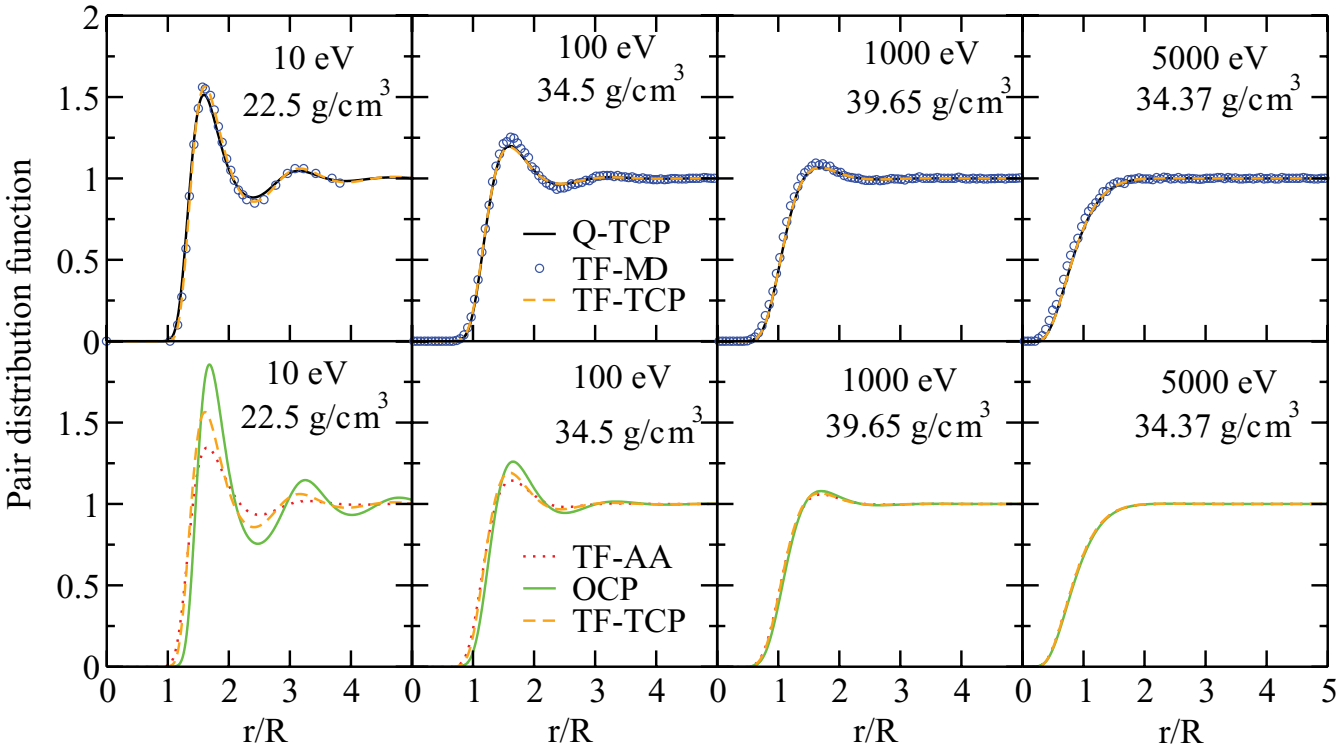

FIG. 5. (Color online) Pair distribution functions $g_{II}(r)$ of iron for conditions along the principal Hugoniot. For the TFAA model $g_{NI}(r)$ is plotted instead. The density and temperature points are taken from Ref. [13]. For the OCP model, the ion charge is taken from the TFTCP model (Table III). The 10 eV TFMD result is from Ref. [50], while the 100, 1000, and 5000 eV TFMD points are from Ref. [13].

good guess for $g_{II}(r)$ to initialize the iterative solution of the full QTCP model.

Finally for aluminum, ion-ion and nucleus-electron pair distribution functions from the quantum model are shown in Fig. 4. For the QTCP an all-electron nucleus-electron pair distribution function can be defined as

$$Zn_I^0 g_{Ne}(r) = n_e^{\rm pa}(r) + n_I^0 \int d\boldsymbol{r}' g_{II}(|\boldsymbol{r} - \boldsymbol{r}'|) n_e^{pa}(r'). \quad (84)$$

This definition of $g_{Ne}(r)$ should be compared to $g_{Ie}(r)$ [Eq. (68)], which only includes the screening electrons $n_e^{\rm scr}(r)$. For small radius the QTCP $g_{Ne}(r)$ becomes large due to the presence of bound states. Oscillations are more pronounced for the lower temperatures and are damped for higher temperatures, echoing the behavior of $g_{II}(r)$. Also shown is the nucleus-electron pair distribution function $g_{Ne}(r)$ from the QAA model [Eq. (71)], which highlights the differences with the QTCP model. The QAA $g_{Ne}(r)$ does not asymptotically go to 1, as the real physically quantity should. While the QAA calculation is all electron in the sense that it accounts for Z electrons around the central nucleus, the electrons belonging to the noncentral ions are not explicitly included in the electron density $n_e(r)$. As noted in Eq. (37), the QAA electron density goes asymptotically to the free electron constant $n_e^0 = Z^\star n_I^0 \neq Zn_I^0$ and $g_{Ne} \to Z^\star/Z \leqslant 1$. This is because there are no field-free electrons in the plasma since far from the central nucleus, electrons move in the field of other ions, as properly described by the QTCP model. Well inside the ion-sphere radius, deeply bound states are not affected by the surrounding plasma and the two nucleus-electron distribution functions are identical, with significant differences only for $r \gtrsim 2$ a.u.

In Fig. 5 ion-ion pair distribution functions for several density-temperature points along the principal Hugoniot of iron are compared to Thomas-Fermi molecular dynamics (TFMD) simulations [13]. These TFMD calculations do not include electron-electron exchange and correlation except for the 10 eV case [50]. The TFTCP results, which all include exchange and correlations, agree very well with the TFMD calculation for all cases. In particular, when exchange and correlations are included for TFMD (10 eV) the agreement becomes excellent. The QTCP results are in good agreement with the TFTCP and TFMD calculations for all cases shown. Only at 10 eV does some difference appear. Note that QMD simulations become computationally prohibitive and impractical for the three highest temperatures shown.

The $g_{II}(r)$ from the OCP model, with the ion charge taken from the TFTCP model, is in good agreement with the other calculations for 1000 and 5000 eV. At 100 eV some difference is seen, and for the 10 eV the OCP model does rather poorly. This is consistent with the results for Al. The agreement of the OCP and TFTCP models could be improved by reducing the ion charge in the OCP model, which highlights the role of the rather arbitrary choice of the ion charge when applying an OCP model to partially ionized warm and hot dense matter where electron screening is significant. The average atom nucleus-ion pair distribution function $g_{NI}(r)$ with the Thomas-Fermi model of the electrons (the TFAA model) is

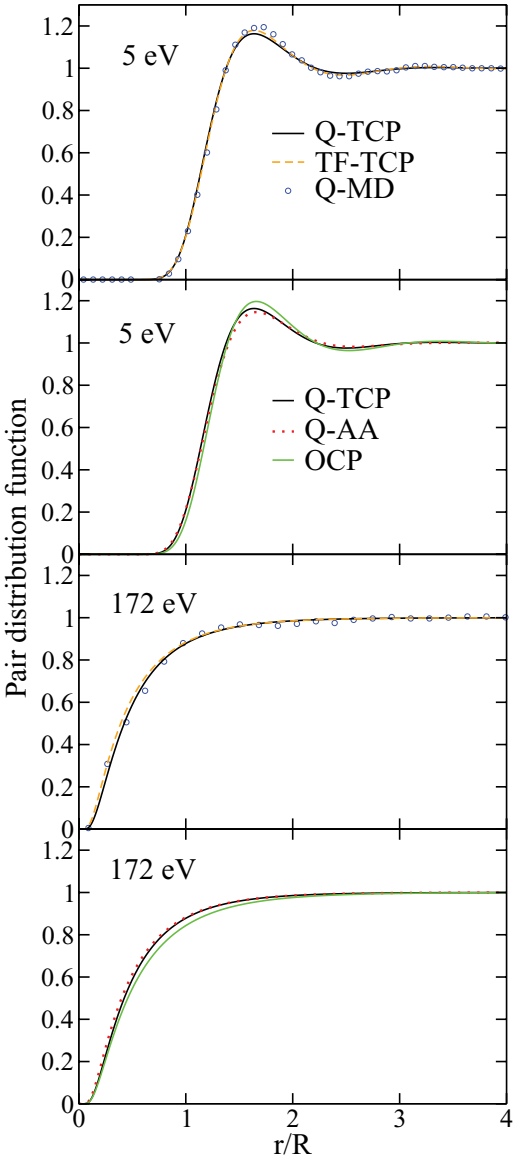

FIG. 6. (Color online) Ion-ion pair distribution functions $g_{II}(r)$ for hydrogen at 80 g/cm^3 and $T = 5$ and 172 eV. The curves labeled QAA show $g_{NI}(r)$ from the average atom model. The QMD data are from Ref. [51].

close to the TFTCP result for the 1000 and 5000 eV cases. For 10 and 100 eV a reduction in correlations in seen.

Calculations for dense hydrogen are shown in Fig. 6 with the corresponding parameters given in Table IV. The agreement between the QTCP, TFTCP, and QMD results is good but not perfect. The relatively small differences are difficult to explain

TABLE IV. Parameters corresponding to the calculations in Figs. 6 and 7 for H at 80 g/cm^3 (n_I^0 =7.08).

T (eV)	$Z^\star$	$\bar{Z}$	$\Gamma_{\rm OCP}$	$\Gamma_{\rm TCP}$
5	0.915	1.00	16.85	7.01
172	0.931	1.00	0.490	0.217

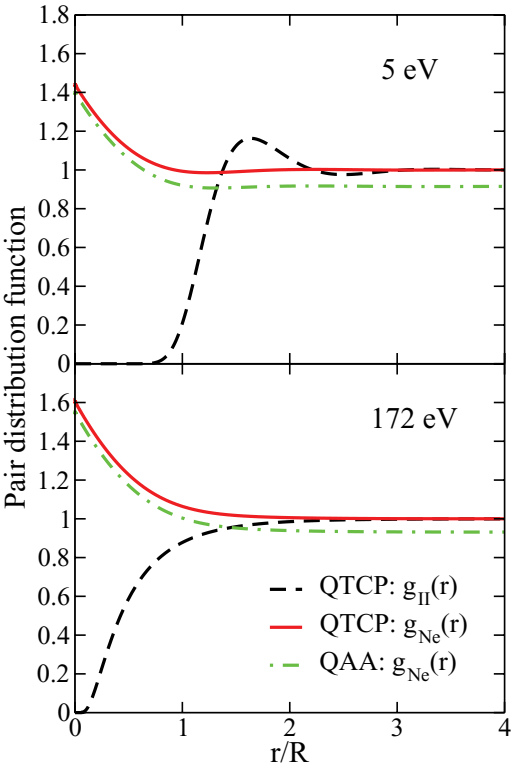

FIG. 7. (Color online) Ion-ion and nucleus-electron pair distribution functions for hydrogen at 80 g/cm^3.

since this is a relatively simple case where for the quantum case no bound states are present [$n_e^{\rm ion}(r) = 0$, Eq. (79)]. The OCP model agrees well with the QMD simulations and, as in the case of Al, the $g_{NI}(r)$ from the QAA model shows slightly weaker correlations than $g_{II}(r)$ in the QTCP model. Since hydrogen is fully ionized at both temperatures, the TFTCP and QTCP models give very nearly identical results. In Fig. 7 the corresponding nucleus electron pair distribution functions

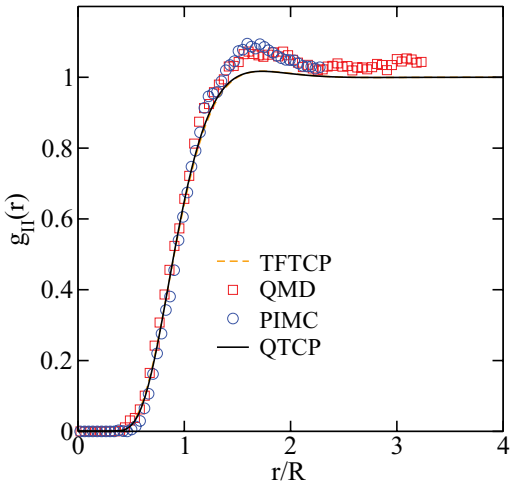

FIG. 8. (Color online) Ion-ion pair distribution functions for carbon at 12.64 g/cm^3 ($n_I^0 = 0.0939$) and $T = 64.64$ eV. The TFTCP and QTCP results overlap almost perfectly. The PIMC and QMD results are from Ref. [16].

are shown. Since there are no bound states, $g_{Ne}(r)$ does not rise sharply near the origin but still shows significant screening of the protons by the electrons.

Finally, in Fig. 8 the QTCP and TFTCP pair distribution functions for carbon are compared to PIMC and QMD calculations [16]. The TF and QTCP models give nearly identical results. Both the PIMC and QMD simulations show stronger correlations than the QTCP model. However, the pair distribution function of the PIMC simulation does not seem to trend asymptotically to 1 at the larger radii shown. It was noted in Ref. [16] that these PIMC and QMD simulations use a small number of particles ($N = 24$) and $g_{II}(r)$ is accurate to $<10\%$, which is enough to explain the differences seen.

V. CONCLUSION

Using the formalism set out in Ref. [22], a model for warm and hot dense matter in which the electronic and ionic structures are calculated self-consistently has been solved numerically. The model couples an average atom model for a central ion to a two-component plasma model of ions and electrons. The local field corrections required by the AA model are provided by the TCP model. In turn, the TCP model is closed with electron densities obtained within the AA model. This method of obtaining the local field corrections is an improvement over the method proposed in Ref. [22]. The coupled equations of the AA and TCP models are solved simultaneously. The inputs to the model are the nuclear charge Z, the temperature T, and the ion particle density n_I^0; there are no free parameters. The ions are treated classically while the electrons can be treated either semiclassically (Thomas-Fermi model) or quantum mechanically (with the Schrödinger equation).

The TCP model is relatively easy to understand from a physical point of view, being a mixture of identical, spherically symmetric ions immersed in a responding quantum electron gas. In contrast, the average atom model is defined by a central nucleus surrounded by spherically averaged electron and ion distributions. The surrounding ions in the average atom model are not the same ions that appear in the TCP model and have in general a different net charge and charge distribution. The average atom ions should not be confused with the usual physical picture of an ion as a nucleus with bound states, surrounded by an interacting cloud of screening electrons. Hence the distinction between the ion charge in the average atom ($Z^\star$) and in the TCP ($\bar{Z}$) models. The recognition of this point lifts unnecessary restrictions found in earlier models (e.g., Ref. [26]) and greatly expands the model's range of validity. In a previous attempt to solve a combination of the TF model of an ion with ion-ion correlations (similar in spirit to the present TFTCP model) [49], solutions could only be found for weakly coupled plasmas. This contrasts with the present method where solutions are found even in the strongly coupled regime and agree very well with TF molecular dynamics simulations.

Numerical results are presented in the form of ion-ion pair distribution functions. Comparisons to Thomas-Fermi and quantum molecular dynamics simulations, as well as path-integral Monte Carlo calculations, show good to excellent agreement for hydrogen, carbon, aluminum, and iron over a wide range of conditions in the warm and hot dense matter regimes. The introduction of an ion-ion bridge function to go beyond the HNC approximation [44] used here should further improve the agreement and extend the validity of the model to simple liquid metals, where ion-ion correlations are very strong.

The main advantage of the present model of warm and hot dense matter over *ab initio* simulations is its relatively low computational cost. Depending on the physical regime, the solution of the model equations for a single density-temperature point is 2–3 orders of magnitude faster than quantum MD simulations. At higher temperatures, QMD simulations become computationally impractical while the QTCP model remains computationally tractable. The QTCP model can be applied at high temperatures where it recovers the TFTCP model. Furthermore, the QTCP model is an all-electron model that does not require the calculation of a pseudopotential and it is not subject to the statistical noise inherent to simulations (e.g., Fig. 8).

The present model is useful for generating pair distribution functions and effective pair potentials that have many uses, including the analysis of x-ray Thomson scattering experiments [8] and the calculation of resistivities [33], as well as for fundamental understanding of the behavior of warm and hot dense matter. This model can form the basis of equation of state calculations and can also be extended to mixtures of ions.

ACKNOWLEDGMENTS

We thank J. A. Anta for sharing his extensive knowledge of the quantum hypernetted chain model of simple liquid metals. We gratefully acknowledge B. Militzer, V. Recoules, F. Lambert, J. D. Kress, and L. Collins for providing pair distribution functions from their *ab initio* simulations. This work was performed under the auspices of the United States Department of Energy under Contract No. DE-AC52-06NA25396.

APPENDIX A: REDUCTION TO AN EFFECTIVE ONE-COMPONENT SYSTEM

Rather than solving the two-component QOZ relations [Eqs. (56) and (57)] in the TCP model directly, the system is reduced to an effective one-component system [39]. Let us assume that there exists a one-component system with pair distribution function $g(r)$ identical to that of the full two-component system $g_{II}(r)$ and that the two systems have the same average density n_I^0,

$$g(r) = g_{II}(r). \tag{A1}$$

By definition

$$g(r) = \exp[-\beta V^{\text{eff}}(r)] \tag{A2}$$

and

$$g_{II}(r) = \exp\left[-\beta V_{II}^{\text{eff}}(r)\right], \tag{A3}$$

where

$$-\beta V^{\text{eff}}(r) = -\beta V(r) + h(r) - C(r) + B(r) \tag{A4}$$

and

$$-\beta V_{II}^{\rm eff}(r) = -\beta V_{II}^{C}(r) + h_{II}(r) - C_{II}(r) + B_{II}(r). \quad \text{(A5)}$$

Here $B(r)$ and $B_{II}(r)$ are bridge functions and $h(r) = g(r) - 1 = h_{II}(r)$. Assuming that

$$B_{II}(r) = B(r), \quad \text{(A6)}$$

it follows that

$$\beta V(r) = \beta V_{II}^{C}(r) - C(r) + C_{II}(r). \quad \text{(A7)}$$

The Ornstein-Zernike equation for a one-component system is

$$C(k) + n_I^0 C(k) h(k) = h(k) \quad \text{(A8)}$$

and for the two-component system

$$C_{II}(k) + n_I^0 C_{II}(k) h_{II}(k) + \bar{n}_e^0 C_{Ie}(k) h_{Ie}(k) = h_{II}(k). \quad \text{(A9)}$$

Since $h(r) = h_{II}(r)$,

$$C(k) - C_{II}(k) = -\frac{\chi_{ee}^0(k) C_{Ie}(k)^2/\beta}{1 + \chi_{ee}^0(k) C_{ee}(k)/\beta} \quad \text{(A10)}$$

$$= n_e^{\rm scr}(k) C_{Ie}(k), \quad \text{(A11)}$$

where

$$n_e^{\rm scr}(k) = -\frac{\chi_{ee}^0(k) C_{Ie}(k)/\beta}{1 + \chi_{ee}^0(k) C_{ee}(k)/\beta} \quad \text{(A12)}$$

and

$$\beta V(k) = \beta V_{II}^{C}(k) - n_e^{\rm scr}(k) C_{Ie}(k). \quad \text{(A13)}$$

This completes the mapping to an effective one-component system. Equation (A13) clearly illustrates the physics of the ion-ion interaction, which is seen to be the sum of the direct Coulomb interaction of point ions and of a screening potential provided by the electron gas. This last term has the form of a linear response of the electron fluid to an external potential $\beta C_{Ie}(k)$, which can also be seen as a electron-ion pseudopotential. It is important to note, however, that the electron response that is embodied in $n_e^{\rm scr}$ and $C_{Ie}(k)$ is computed from the solution of the Schrödinger (or Thomas-Fermi) equation and is thus highly nonlinear. The linear response formalism in a model such as the screened one-component plasma [42] can be recovered readily from the present model.

The one-component Ornstein-Zernike equation (A8) and the closure relation [Eq. (A2)] are solved with this effective one-component potential for the pair correlation function $h(r)$ and the direct correlation function $C(r)$, which gives $h_{II}(r)$ by Eq. (A1) and the ion density $n_I(r)$ with Eq. (70). The only approximation involved in this mapping is the equality of the bridge functions of the two systems [Eq. (A6)].

APPENDIX B: ION-SPHERE MODEL

The ideal electron chemical potential [Eqs. (15), (21), and (40)] is evaluated within a simplified version of the average atom model presented above where the ion distribution is chosen to be

$$n_I(r) = n_I^0 \Theta(r - R), \quad \text{(B1)}$$

where Θ is the Heaviside step function. In the context of the coupled average atom and two-component models with ion correlations, this simpler model provides an approximate $\mu_e^{\rm id}$ [Eq. (40)] and a surprisingly good guess for $n_e^{\rm scr}(r)$ to initialize the numerical solution of the problem. A more rigorous determination of $\mu_e^{\rm id}$ is beyond the scope of the present paper.

The electronic density $n_e(r)$ is obtained by solving the Thomas-Fermi equation (24) or the Schrödinger equation (17) with the effective potential

$$V_{Ne}^{\rm eff}(r) = -\frac{Z}{r} + \int \frac{[n_e(r') - n_e^0 \Theta(r' - R)] d\boldsymbol{r}'}{|\boldsymbol{r} - \boldsymbol{r}'|} + V_{ee}^{\rm xc}[n_e(r)] - V_{ee}^{\rm xc}[n_e^0], \quad \text{(B2)}$$

where global neutrality of the plasma has been imposed. A second neutrality condition

$$Z = \int_{r<R} n_e(r) d\boldsymbol{r} \quad \text{(B3)}$$

(i.e., neutrality of the ion sphere) gives the electron chemical potential $\mu_e^{\rm id}$ [Eq. (16)]. In contrast to Eq. (54), the potential (B2) does not involve the local field corrections since the surrounding ions are no longer correlated, given Eq. (B1). The electron exchange and correlation potential $V_{ee}^{\rm xc}$ is approximated using the simple Dirac exchange functional [38], as it is for all calculations presented here. This model is similar to the INFERNO model [20] and identical to the neutral Wigner-Seitz model of Ref. [52] provided the same exchange treatment is used. In its Thomas-Fermi version, this model is identical to that in Ref. [19].

As described in Sec. III, the electron density attributed to the external plasma $n_e^{\rm ext}(r)$ [Eq. (74)] is obtained by solving the Schrödinger (or Thomas-Fermi) equation with the same effective potential as in Eq. (B2) but without the central nucleus (with the same $\mu_e^{\rm id}$ however)

$$V_e^{\rm eff,ext}(r) = \int \frac{[n_e^{\rm ext}(r') - n_e^0 \Theta(r' - R)] d\boldsymbol{r}'}{|\boldsymbol{r} - \boldsymbol{r}'|} + V_{ee}^{\rm xc}[n_e^{\rm ext}(r)] - V_{ee}^{\rm xc}[n_e^0]. \quad \text{(B4)}$$

This allows $n_e^{\rm scr}$ to be determined, providing an initial guess for the local field corrections [Eq. (67)]. As reported in Sec. IV, this initial estimate works rather well (Fig. 3). The models of Refs. [4,23] as well as the jellium vacancy model of Ref. [53] are similar to this model.

APPENDIX C: BROADENING OF BOUND STATES

In Ref. [54] it was proposed that the inverse of the average relaxation time $(1/\tau)$ for the scattering electron states could give a reasonable estimate of the observed broadening of bound-bound transitions in spectra by accounting for dense plasma effects. This hypothesis has been confirmed numerically [55,56]. This estimate of the state broadening in dense matter is used to obtain a definition of an ion for the quantum mechanical case that is continuous as a function of density and temperature [Eq. (79)]. The level broadening in Eq. (81) is set to $\gamma = 1/\tau$ for all bound states.

Following Ref. [57], the average relaxation time τ is related to the dc conductivity $\sigma_{\rm dc}$ via the Drude formula

$$\tau = \frac{\sigma_{\rm dc}}{n_e^0}, \quad \text{(C1)}$$

where n_e^0 is calculated from the electron chemical potential $\mu_e^{\rm id}$ [Eq. (40)]. The dc conductivity can be calculated from the momentum-dependent relaxation time $\tau(k)$ from the Ziman formula

$$\sigma_{\rm dc} = \frac{2}{3}\int \frac{d\mathbf{k}}{(2\pi)^3}\left(-\frac{\partial g_k}{\partial \epsilon}\right) v^2 \tau(k), \tag{C2}$$

where g_k is the Fermi occupation factor [Eq. (15)], $v = \sqrt{2\epsilon}$ is the electron velocity, and $\tau(k)$ is related to the momentum transport cross section $\sigma_{\rm tr}$,

$$\tau(k) = \frac{\sigma_{\rm tr}(k)}{n_I^0 v}. \tag{C3}$$

Finally, $\sigma_{\rm tr}$ is found from the average atom phase shifts δ_l,

$$\sigma_{\rm tr}(k) = \frac{4\pi}{k^2}\sum_{l=0}^{\infty}(l+1)[\sin(\delta_{l+1}-\delta_l)]^2 \tag{C4}$$

and l is the orbital angular momentum quantum number. In practice only a small number of terms are required as the summation converges rapidly.

[1] US Department of Energy report http://science.energy.gov/~/media/fes/pdf/workshop-reports/Hedlp_brn_workshop_report_oct_2010.pdf, 2009 (unpublished).
[2] B. A. Hammel, S. W. Haan, D. S. Clark, M. J. Edwards, S. H. Langer, M. M. Marinak, and M. V. Patel, High Energy Density Phys. **6**, 171 (2010).
[3] *The Equation of State in Astrophysics: IAU Colloquium 147*, edited by G. Chabrier and E. Schatzman (Cambridge University Press, Cambridge, 1994).
[4] O. Peyrusse, J. Phys.: Condens. Matter **20**, 195211 (2008).
[5] A. Mancic *et al.*, Phys. Rev. Lett. **104**, 035002 (2010).
[6] V. Recoules and S. Mazevet, Phys. Rev. B **80**, 064110 (2009).
[7] E. G. Saiz *et al.*, Nat. Phys. **4**, 940 (2008).
[8] A. L. Kritcher *et al.*, Science **322**, 69 (2008).
[9] O. Ciricosta *et al.*, Phys. Rev. Lett. **109**, 065002 (2012).
[10] S. Mazevet, M. P. Desjarlais, L. A. Collins, J. D. Kress, and N. H. Magee, Phys. Rev. E **71**, 016409 (2005).
[11] M. P. Desjarlais, J. D. Kress, and L. A. Collins, Phys. Rev. E **66**, 025401(R) (2002).
[12] G. Zérah, J. Clérouin, and E. L. Pollock, Phys. Rev. Lett. **69**, 446 (1992).
[13] F. Lambert, J. Clerouin, and G. Zerah, Phys. Rev. E **73**, 016403 (2006).
[14] F. Lambert, V. Recoules, A. Decoster, J. Clerouin, and M. Desjarlais, Phys. Plasmas **18**, 056306 (2011).
[15] D. M. Ceperley, Rev. Mod. Phys. **67**, 279 (1995).
[16] K. P. Driver and B. Militzer, Phys. Rev. Lett. **108**, 115502 (2012).
[17] L. H. Thomas, Proc. Cambridge Philos. Soc. **23**, 542 (1927).
[18] E. Fermi, Z. Phys. **48**, 73 (1928).
[19] R. P. Feynman, N. Metroplis, and E. Teller, Phys. Rev. **75**, 1561 (1949).
[20] D. A. Liberman, Phys. Rev. B **20**, 4981 (1979).
[21] B. Wilson, V. Sonnad, P. Sterne, and W. Isaacs, J. Quantum Spectrosc. Radiat. Transfer **99**, 658 (2006).
[22] C. E. Starrett and D. Saumon, Phys. Rev. E **85**, 026403 (2012).
[23] F. Perrot, Phys. Rev. A **42**, 4871 (1990).
[24] J. M. Ziman, Proc. Phys. Soc. **91**, 701 (1967).
[25] L. Dagens, J. Phys. C **5**, 2333 (1972).
[26] J. Chihara, J. Phys.: Condens. Matter **3**, 8715 (1991).
[27] K.-C. Ng, J. Chem. Phys. **61**, 2680 (1974).
[28] J.-P. Hansen, Phys. Rev. A **8**, 3096 (1973).
[29] G. S. Stringfellow, H. E. DeWitt, and W. L. Slattery, Phys. Rev. A **41**, 1105 (1990).
[30] G. Gregori, A. Ravasio, A. Höll, S. H. Glenzer, and S. J. Rose, High Energy Density Phys. **3**, 99 (2007).
[31] V. Schwarz, Th. Bornath, W.-D. Kraeft, S. H. Glenzer, A. Höll, and R. Redmer, Contrib. Plasma Phys. **47**, 324 (2007).
[32] W. R. Johnson, J. Nilsen, and K. T. Cheng, Phys. Rev. E **86**, 036410 (2012).
[33] F. Perrot and M. W. C. Dharma-wardana, Phys. Rev. A **36**, 238 (1987).
[34] D. E. Hanson, L. A. Collins, J. D. Kress, and M. P. Desjarlais, Phys. Plasmas **18**, 082704 (2011).
[35] T. Blenski and K. Ishikawa, Phys. Rev. E **51**, 4869 (1995).
[36] J. Clérouin, E. L. Pollock, and G. Zerah, Phys. Rev. A **46**, 5130 (1992).
[37] D. A. Liberman, J. Quantum Spectrosc. Radiat. Transfer **27**, 335 (1982).
[38] P. A. M. Dirac, Proc. Cambridge Philos. Soc. **26**, 376 (1930).
[39] J. A. Anta and A. A. Louis, Phys. Rev. B **61**, 11400 (2000).
[40] J.-P. Hansen and I. R. McDonald, *Theory of Simple Liquids*, 3rd ed. (Academic, New York, 2006).
[41] S. Ichimaru, *Statistical Plasma Physics, Volume II: Condensed Plasmas* (Westview, Boulder, 2004).
[42] G. Chabrier, J. Phys. France **51**, 1607 (1990).
[43] G. Faussurier, Phys. Rev. E **69**, 066402 (2004).
[44] Y. Rosenfeld, J. Stat. Phys. **42**, 437 (1986).
[45] H. Iyetomi, S. Ogata, and S. Ichimaru, Phys. Rev. A **46**, 1051 (1992).
[46] W. Daughton, M. S. Murillo, and L. Thode, Phys. Rev. E **61**, 2129 (2000).
[47] J. Chihara, J. Phys. C: Solid State Phys. **17**, 1633 (1984).
[48] J. K. Percus, Phys. Rev. Lett. **8**, 462 (1962).
[49] D. Ofer, E. Nardi, and Y. Rosenfeld, Phys. Rev. A **38**, 5801 (1988).
[50] J. D. Kress and L. A. Collins (private communication).
[51] V. Recoules, F. Lambert, A. Decoster, B. Canaud, and J. Clérouin, Phys. Rev. Lett. **102**, 075002 (2009).
[52] R. Piron and T. Blenski, Phys. Rev. E **83**, 026403 (2011).
[53] J. Chihara, Phys. Rev. A **40**, 4507 (1989).
[54] W. R. Johnson, C. Guet, and G. F. Bertsch, J. Quantum Spectrosc. Radiat. Transfer **99**, 327 (2006).
[55] J. Clérouin, C. Starrett, P. Noiret, P. Renaudin, C. Blancard, and G. Faussurier, Contrib. Plasma Phys. **52**, 17 (2012).
[56] J. Clérouin, C. Starrett, G. Faussurier, C. Blancard, P. Noiret, and P. Renaudin, Phys. Rev. E **82**, 046402 (2010).
[57] W. R. Johnson, High Energy Density Phys. **5**, 61 (2009).